 https://doi.org/10.3311/PPme.23482

Periodica Polytechnica Mechanical Engineering, 67(4), pp. 350–360, 2023

Investigating Particle Paths in Intracranial Aneurysms: A Parametric Study

Dániel Gyürki[1*], György Paál[1]

[1] Department of Hydrodynamic Systems, Faculty of Mechanical Engineering, University of Technology and Economics, Műegyetem rkp. 3., H-1111 Budapest, Hungary
[*] Corresponding author, e-mail: dgyurki@hds.bme.hu

Received: 20 September 2023, Accepted: 30 October 2023, Published online: 09 November 2023

Abstract

A large part of computational fluid dynamics (CFD) studies in hemodynamics concentrates on the berry-like bulgings on cerebral vessel walls, called intracranial aneurysms (IA). One technique is the calculation of particle paths, which can help understand important physiological processes like thrombus formation or drug propagation. The problem is that the particle paths can display chaotic nature even in simple flows, thus, investigating the effects of parameters on the particle paths is essential. The method used in this study consists of four steps. The first step is to voxelize the observed domain into a uniform voxel grid, the second step is to simulate the velocity flow field using the lattice-Boltzmann method, then to calculate one million particle paths using a fourth-order Runge-Kutta integrator. Lastly, the final step is the calculation of the relative perimeter, relative area and their ratio (P/A ratio) for each outlet when the particle release plane is colored according to the outlets the particles took. Five patient-specific cases were investigated. After a voxel size and integrator time step dependence study, the effect of the presence of the aneurysm sack and the particle release time within the heart cycle were assessed. Based on five geometries, the presence of the aneurysm sac increases the P/A ratio (which is a direct link to the chaotic nature of the particle paths), and when the particles are released near the peak and the decelerating phase of the heart cycle, the P/A ratio also significantly increases.

Keywords

aneurysm, particle path, lattice-Boltzmann simulation, chaotic nature

1 Introduction

Computational fluid dynamics (CFD) is used by an ever-growing part of the fluid mechanics research community since more and more computational resources are becoming generally available. The same applies to the area of hemodynamics. The two main types of treating hemodynamic problems are one-dimensional and three-dimensional simulations. The former concentrate on the whole circulatory system, or just on the arterial or venous system. The aim of such research is to model certain effects globally on the whole system [1, 2], create a database from virtual patients to assess the variability in human cardio vasculature [3], or couple the global simulation with local 3D simulations [4]. On the other hand, 3D simulations are performed mainly locally on a smaller part of the arterial or venous system. At most times, these studies deal with various vessel wall malformations, like stenoses (narrowing) [5, 6] or aneurysms [7].

Aneurysms are local dilatations/bulges of the arterial walls, located primarily on the abdominal artery or certain intracranial arteries. Intracranial aneurysms (IA) are present in the form of a berry-like bulge on the vessel walls, mainly the vessels of the Circle of Willis [8]. IAs are generally asymptomatic. However, the main concern with these malformations is the danger of rupture, which causes subarachnoid hemorrhage (SAH), and the patient may remain dependent (~33%) or die in half of the cases [9].

IAs are a widely researched topic. CFD studies may focus on the initiation of IAs [10–13], while numerous papers deal with their treatment methods, for example, the use of flow diverters [14–16]. The aim of these studies can also be to find the development of an aneurysm leading to the rupture or the effect of an aneurysm on the flow itself [17, 18]. One part of these studies concentrate on fictive particles or ink released in the flow domain, and calculate their paths or concentration.

Particle residence times (PRT) were calculated by Leemans et al. [19] and were correlated with morphology

Cite this article as: Gyürki, D., Paál, G. "Investigating Particle Paths in Intracranial Aneurysms: A Parametric Study", Periodica Polytechnica Mechanical Engineering, 67(4), pp. 350–360, 2023. https://doi.org/10.3311/PPme.23482

and the ruptured state of IAs. While morphology has an important effect on PRT, correlation with the ruptured state is insignificant. Calculating particle paths can also model other vital aspects of human physiology, for example, thrombus deposition in geometries [20, 21] or particles travelling with the blood flow during drug administration [22, 23]. Meschi et al. [24] concentrate on targeted drug delivery in diseased regions of the arteries, which relies heavily on particle path calculations.

However, it is important to note that particle paths in 3D can become chaotic, even in the case of simple flows [25, 26]. Závodszky et al. [27] found that particles show chaotic nature when placed inside perianeurysmal flow. Fractal-like patterns emerge because of the chaotic advection of the particles when projected back on the release plane and colored according to PRT. 2D flows can also exhibit similar features. Silva et al. [28] observed chaotic advection in carotid bifurcation simulations. One reason behind this phenomenon may be the fact that even though the flow is laminar in the cerebral arteries in most cases, some researchers found that instabilities may arise during certain parts of the cardiac cycle, dominantly in the decelerating phase [29, 30]. Since particle paths may differ if released at different points of the heart cycle, Suh et al. [31] divided the heart cycle into 10 intervals and then averaged the PRTs of the particles released at the start of each interval.

According to Tambasco and Steinman [32], Lagrangian particle tracking is computationally expensive, as high mesh resolution is needed to accurately track the particles in complex flows. This finding agrees with Závodszky et al. [27]. Therefore, an Eulerian approach is proposed instead of Lagrangian tracking [33–35]. Reza and Arzani [36] performed a thorough study calculating and correlating six widely used residence time metrics. Their conclusion is to find the appropriate one based on the application.

In this study, which is an extension of the author's previous work [37], the particle paths are calculated in five patient-specific geometries. The first aim is a dependence study, where the effect of the refinement of the voxel size and integrator time step size is investigated on the particle paths. Then, the effect of the presence of the aneurysm sac and the particle release time is observed on the particle paths.

2 Methods

2.1 Geometry preparation

The procedure used during this research starts with obtaining the geometry and preparing it for the simulations. The medical partners provide patient-specific medical images in DICOM format taken with 3D digital subtraction angiography (DSA). The data acquisition was conducted according to the principles expressed in the Declaration of Helsinki. All patients provided written informed consent. After segmenting the images with Slicer 3D [38], the STL geometries are further refined using the open-source software called MeshLab [39]. The 3D geometries were processed based on previous experiences and consultations with neurointerventionalists.

The following step is to create straight pipe sections at each opening of the geometries. These extensions provide enough space to make the effects of the imposed boundary conditions during simulations negligible. Then, the geometries are rotated and box-cut in a way that the inlet of the observed domain is parallel with the XY plane. These geometrical transformations were performed using an in-house script written in Python.

The next step in preparing the geometries for the simulations is to generate a voxel field. The whole bounding box of the geometry is divided into a uniform hexahedral grid, described with only one parameter, the voxel size. Each voxel is then assigned a value, based on which it is either unused (not part of the flow field), fluid, wall or opening (used for boundary conditions) voxels. The voxelization is performed using an in-house Python code. Five patient-specific aneurysm geometries were investigated in this preliminary study, see Fig. 1 (Case1 to Case5).

The first part of this study concentrates on finding the optimum voxel size. If the voxel size is too large, the small details, especially the chaotic nature of the flow, are lost because of the poor discretization. However, if the voxel size is too small, the whole procedure becomes computationally demanding, even on supercomputers. Four different voxel sizes were used during this research for each geometry so that the total voxel number of the whole domain is around 50, 100, 150 and 200 million. The time integrator was kept constant at the finest value.

2.2 Obtaining the velocity field

The fluid flow simulations can be performed after the voxel field is ready. The simulations are based on the lattice-Boltzmann method (LBM). The LBM originates in the lattice gas automaton to solve fluid flow problems. Instead of solving the Navier-Stokes equations directly, like the finite volume method does, the LBM calculates the collision and streaming of fictive particles. The macroscopic quantities, which are usual in fluid flow simulations, like velocity or pressure, are calculated based

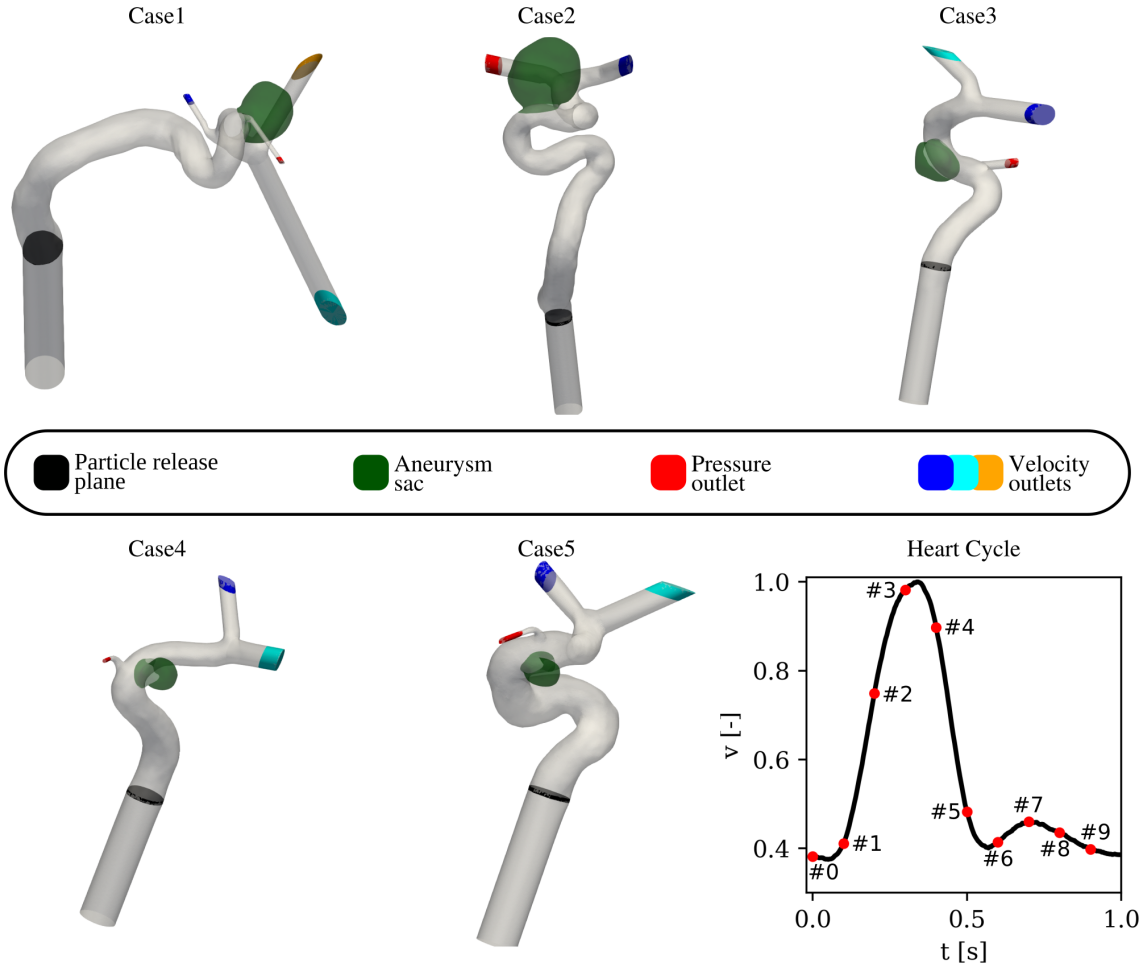

Fig. 1 The five geometries used in this research (black: particle release plane; green: aneurysm sac; red: pressure outlet; blue, cyan and orange: velocity outlets) and the inlet heart cycle signal (bottom right corner)

on probability density functions of the fictive particles. The LBM can be performed on a uniform grid only, hence the box-cut and the uniform voxelization mentioned in the previous subsection.

A parabolic velocity boundary condition is prescribed at the inlet of the domain. A generalized, synthetic 1 s long carotid artery velocity cycle signal, which was used in previous studies [27, 40], modulates the maximum of the parabola. The signal can be seen in the bottom right corner in Fig. 1. At the peak of the cycle, the Reynolds number, based on the cross-sectional average velocity at the inlet is chosen to be 250 for every case. This value is physiologically plausible in the observed artery segment, which could be made patient-specific based on the inlet diameter in later studies.

The smallest outlet is prescribed as a static pressure outlet with 0 Pa to avoid over-constraining the simulation (colored red in Fig. 1). The other outlets are velocity outlets with parabolic velocity profiles (colored blue, cyan and orange). The velocities at each outlet are calculated based on Murray's law [41], which divides the volumetric flow rates proportionally to the second power of the areas of the outlets. Lastly, the bounce-back scheme is prescribed at the voxels assigned with the wall flag during voxelization.

The flow simulations were transient (time-dependent), the time step is determined according to the stability criterion of the LBM and depends on the voxel size. The time step was around 10^{-5} seconds, and the velocity field was saved at every 0.01 second, resulting in 100 flow fields for the one-second-long heart cycle.

The simulations were performed using an in-house code written in C++ which is based on the open-source code package Palabos [42]. The main advantage of the LBM is the potential of high-degree parallelization. This means that the simulation can be performed on high-performance computers, so that the computational time is reduced, compared to simulations using the finite volume method [43–45].

2.3 Calculating the particle paths

After obtaining the velocity fields, the next step is to calculate the paths of different particles placed in the flow field. The particles or tracers are considered massless, so they instantaneously take on the velocity of a given point in the flow field (Eq. (1)) and are passive, so they do not affect the flow itself. As for now, the particles are not representing any physiological processes, but in further projects it is possible to modify our methods in order to represent targeted drug delivery or thrombus formation.

The velocity field has to be integrated along the particle path from a starting position to acquire the position of a given particle at a given time, see Eq. (2).

$$\dot{\boldsymbol{r}}(t) = \frac{d\boldsymbol{r}(t)}{dt} = \boldsymbol{v}\left(\boldsymbol{r}(t), t\right), \tag{1}$$

$$\boldsymbol{r}(t) = \int_{t_0}^{t} \boldsymbol{v}\left(\boldsymbol{r}(t'), t'\right) dt' + \boldsymbol{r}(t_0), \tag{2}$$

where $\boldsymbol{r}(t)$ is the position vector of a particle at time t, $\boldsymbol{v}(\boldsymbol{r}(t), t)$ is the velocity vector at position $\boldsymbol{r}(t)$ and $\boldsymbol{t}_0$ is the particle release time.

The integrations were performed using a fourth-order Runge-Kutta method with a fixed time step. The integrator is an in-house code written in C++. The integration is done for 10 seconds (10 heart cycles) to allow enough time for the particles to leave the observed domain. There are two outputs for each particle, a particle residence time (PRT) and an outlet. The first one is the time it takes the particle to leave the domain, while the second one is the outlet through which it leaves. The calculations are performed for one million particles released near the inlet of the original geometry (indicated with a black plane in Fig. 1).

In this preliminary study, the effect of the time step of the integrator is investigated. If the time step is too large, the particles may jump over important aspects of their paths, while if the time step is too small, it would take too much time to perform the integration. Three different time steps were used: 0.001 s, 0.0005 s and 0.0001 s, while the voxel size was the finest (200M mesh).

2.4 Effect of the aneurysm sac/particle release time

As mentioned previously, one part of this paper is finding the optimum values for the voxel size and the integrator time step. The other aim of this research is to perform a preliminary investigation on the effect of the presence of the aneurysm sac and the particle release time during the heart cycle with respect to the paths of the particles.

The pre-aneurysm geometry is artificially but objectively generated by removing the aneurysm sac. The method is similar to the one described by Csippa et al. [13]. The sacs are colored green in Fig. 1. All other settings of the simulations and calculations are the same for the pre-aneurysm and post-aneurysm cases, therefore only the effect of the presence of the aneurysm sac itself is imposed on the particle paths. The consequence of different particle release times during the heart cycle is investigated by defining 10 equidistant time instances in the heart cycle (red dots on the heart cycle curve in Fig. 1) and starting the path calculations at those time instances from the release plane near the inlet (black plane in Fig. 1).

In order to compare the different scenarios, the PRTs and outlets, through which the particles leave are further processed. The outlets belonging to each particle are recorded and projected back to the release plane. This plane is colored according to the outlet through which the particle starting from that point leaves the domain (the outlet colors match those in Fig. 1). Then the next step is to summarize the perimeter and area of the regions corresponding to one outlet. These sums are normalized with the perimeter and area of an area-equivalent circle to the cross-section of the releasing plane. Obviously, the area corresponding to each outlet is always finite. However, if the resulting particle paths become increasingly chaotic, they display a filamentary structure when projected onto the particle releasing plane, so the respective perimeter grows. Therefore, the perimeter to area ratio (P/A ratio) for a given outlet will grow as the particle paths become more chaotic. This way, the effects of the sac or the release time can be qualitatively and quantitatively estimated.

As the values for the P/A ratio are calculated, based on the data of the whole cross section, they fully represent the geometry and the flow itself. The advantage of the P/A ratio is the simple calculation method and the global representation of a geometry, while the usual metrics, like the fractal dimension are more computationally demanding and can be problematic in the case of real-life data. The resolution-dependence of the P/A ratio is eliminated here by comparing results to each other and observing only tendencies.

3 Results and discussion

3.1 Mesh and integrator time step dependence

The mesh and integrator time step dependence simulations were performed for all five cases but only for the geometries with the aneurysms. The particles were released at

the start of the heart cycle (instant #0 in Fig. 1). Fig. 2 shows the particle release plane colored according to the outlet through which the particle originating from that point leaves the domain for Case1. The colors match those in Fig. 1. The three subfigures are the results of the three simulations with different time steps. Similar diagrams could be drawn from the mesh dependence simulations.

Based on the method described in Subsection 2.4, the results are condensed to make them comparable. The data shown in Fig. 2 are processed and displayed in Fig. 3, where the relative perimeter, relative area and their ratio can be seen for each outlet and for the three different integrator time steps. The last diagram is a relative percentage error of the P/A ratio compared to an extrapolated value. The extrapolated value is calculated based on the three different simulations, and was obtained according to Celik et al. [46]. This method is used for calculating an extrapolated value with an infinitely fine voxel size based on three simulations with different resolutions.

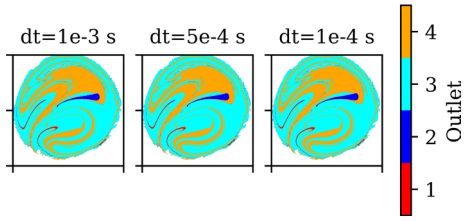

Fig. 2 The results of the integrator step dependence study for Case1 started at instant #0. The inlet plane is colored according to the outlets through which the particles leave the domain

A similar figure can be constructed based on the results of the mesh dependence calculations, which can be seen in Fig. 4 for Case 1. In both figures, the relative error of 5% is indicated with a dotted line. Apart from four, every perimeter/area ratio reaches this 5% error value during the refinement of the voxel size or the integrator time step.

The perimeter/area ratio values for each outlet from Case1 to Case5 can be found in Table 1 for the mesh dependence simulations, and in Table 2 for the integrator time step dependence ones. It is visible in the first column of Table 2 that, in one third of the cases, the ratio values obtained with the largest integrator time step are very distinctive compared to the values calculated with finer time steps. This means that the particles "jump over" some important aspects of the flow in time using the largest applied time step size. Similar tendencies can be seen in Table 1, where the voxelization is not fine enough, the velocity field, and as a result, the particle paths lack the fine details. The results in Tables 1 and 2 show that in most simulations the mesh and integrator time step independence is reached with the 200 million cell number and the time step of 1e-4 s, if the extrapolated value based on the Richardson extrapolation technique mentioned in [46] is considered exact. Therefore, these values are used in the next part of the study. If the mesh and integrator time step dependence is calculated based on the perimeters or the area, the relative errors are smaller on average than the relative error of the P/A ratio.

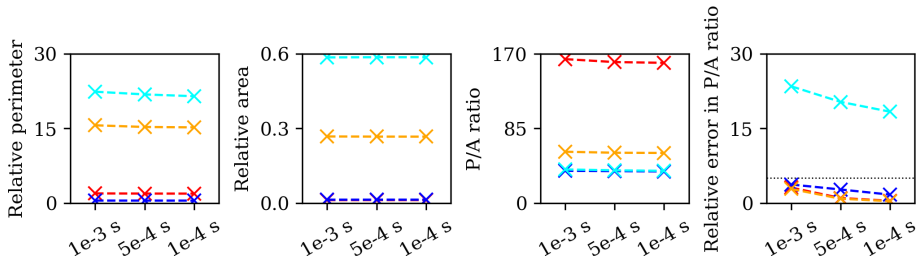

Fig. 3 Relative perimeter, relative area, their ratio and its relative error of each outlet for Case1 in the case of the integrator time step dependence calculations with the finest voxel size (200M mesh) started at instant #0. The colors of the outlets match those in Fig. 1 and Fig. 2

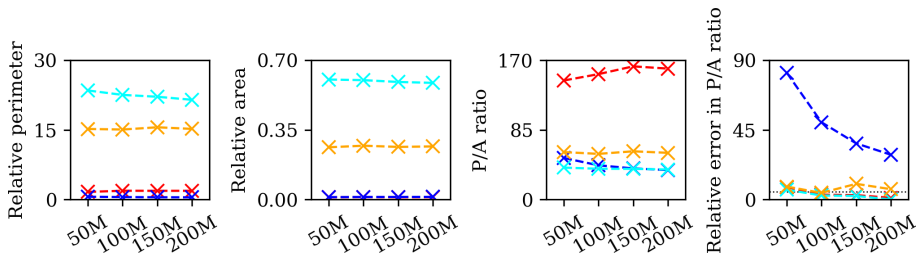

Fig. 4 Relative perimeter, relative area, their ratio and its relative error of each outlet for Case1 in the case of the mesh dependence calculations with the finest integrator time step (*dt* = 1e-4 s) started at instant #0. The colors of the outlets match those in Figs. 1 and 2

Table 1 The ratio of the perimeter and area of the particles corresponding to each outlet. The results show the mesh dependence study (with the finest integrator time step), the last column is the extrapolated value based on the three finest meshes

Case	Outlet color	Mesh				Extrap. value
		50M	100M	150M	200M	
1	Red	145.1	152.9	162.4	159.6	157.9
	Blue	50.7	41.8	38.0	35.9	27.9
	Cyan	39.0	37.6	37.5	36.6	36.6
	Orange	57.9	55.7	58.8	57.0	53.4
2	Red	75.0	77.7	68.1	71.8	75.1
	Blue	69.7	61.8	65.6	68.4	108.6
3	Red	8.9	8.8	8.1	8.0	7.9
	Blue	27.4	25.0	8.6	8.7	8.7
	Cyan	32.6	31.8	14.1	14.2	14.2
4	Red	24.3	23.0	22.8	22.8	22.8
	Blue	18.7	17.6	17.1	17.1	17.1
	Cyan	6.2	5.6	5.4	5.6	6.4
5	Red	19.8	18.3	10.4	9.8	9.7
	Blue	13.2	11.7	10.2	9.1	7.9
	Cyan	14.7	13.9	5.6	5.0	4.8

Table 2 The ratio of the perimeter and area of the particles corresponding to each outlet. The results show the integrator time step dependence study (with the finest voxel size), the last column is the extrapolated value based on the three time steps

Case	Outlet color	*dt*			Extrap. value
		1e-3 s	5e-4 s	1e-4 s	
1	Red	163.9	160.5	159.6	158.9
	Blue	36.7	36.3	35.9	35.3
	Cyan	38.2	37.2	36.6	31.0
	Orange	58.4	57.3	57.0	56.8
2	Red	73.2	72.4	71.8	69.3
	Blue	68.7	68.4	68.4	68.3
3	Red	105.7	7.9	8.0	8.0
	Blue	80.7	8.7	8.7	8.7
	Cyan	14.0	13.9	14.2	14.4
4	Red	56.0	22.3	22.8	22.8
	Blue	20.3	16.9	17.1	17.1
	Cyan	104.1	5.6	5.6	5.6
5	Red	10.3	10.2	9.8	9.7
	Blue	14.2	11.0	9.1	7.5
	Cyan	6.1	5.3	5.0	3.8

3.2 Effect of the aneurysm sac/particle release time

The second part of this research is a study with these five cases to reveal the effect of the aneurysm sac and the particle release time within the heart cycle on the particle paths. For each case and each version (with or without aneurysm), ten calculations were performed with different particle release times, as mentioned in Subsection 2.4. Every simulation setting is the same, only the presence of the aneurysm sac or the particle release time is different. The results can be seen in Fig. 5 for Case3 with the aneurysm sac still on. Similar figures could be made for the other cases and versions as well.

It can be easily seen in Fig. 5 that the areas corresponding to different outlets display drastically different natures in the different subplots. While the result of the release instant #0 shows easily distinguishable, simple areas between the three outlets, the plots corresponding to other release times during the heart cycle display a more complex, filamentary structure (e.g. #3, #4 and #5). The simpler, well-defined areas resume if the particles are released later in the heart cycle (e.g. #7, #8 and #9). The aforementioned relative perimeter, relative area and their ratio are calculated for each particle release time and for the version without the aneurysm sac as well. These can be seen in Fig. 6. The top row is without the aneurysm, while the bottom row is the version with the aneurysm. The different particle release times are on the horizontal axes.

The middle column of Fig. 6 shows that within certain limits, the relative area does not vary much, and it is a bounded value, it cannot be larger than 1. The values are similar in both versions, so an aneurysm does not have a significant effect on the particle path outlet areas. In contrast, the relative perimeter corresponding to the outlets varies significantly with respect to the particle release time and with the presence of the aneurysm. Therefore, the perimeter per area ratio is calculated for each case, which is the third column in Fig. 6.

Fig. 6 shows that the particles released near the peak of the heart cycle, the P/A ratio will increase significantly. As mentioned in the introduction, some studies found that instabilities may appear in the flow during deceleration. Therefore, it is hypothesized that if the particles are present in the observed domain during the decelerating phase, the plots like Fig. 5 will display the filamentary, chaotic picture, and as a result, the P/A ratio will increase. The ratio will decrease again, when the particles are released at the nearly constant phase of the heart cycle.

If the two rows of Fig. 6 are compared, the effect of the aneurysm can be seen. As previously mentioned, the relative area is similar in both versions. However, the relative perimeter, and as a result the P/A ratio is significantly different in the two versions. The extent of the P/A ratio

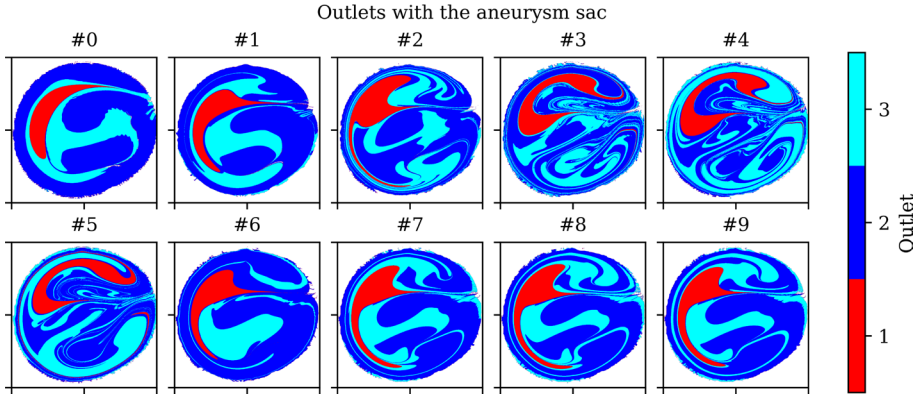

Fig. 5 The results of the different particle release times for Case3. The inlet plane is colored according to the outlets through which the particles leave the domain. The colors of the outlets match those in Fig. 1

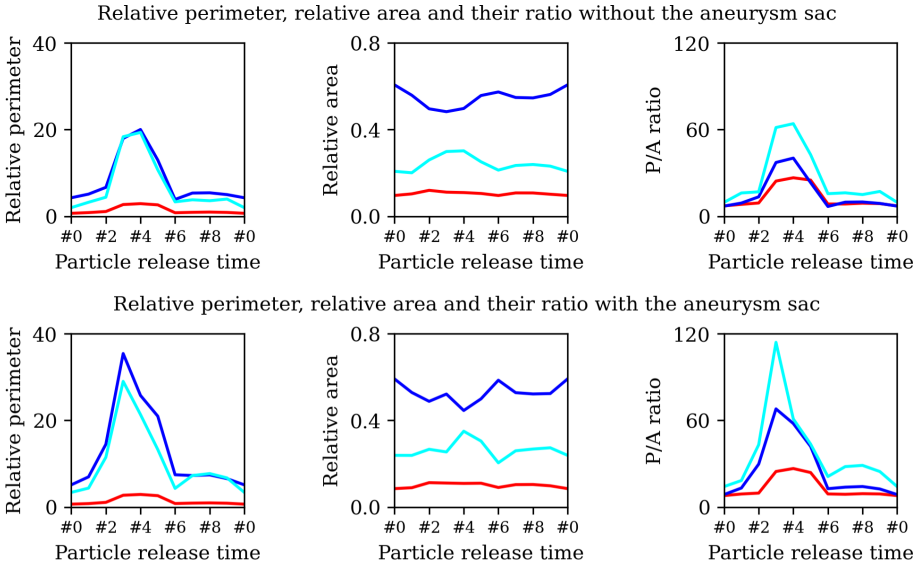

Fig. 6 Relative perimeter, relative area and their of each outlet for Case3 without (top) and with aneurysm (bottom) as the function of particle release time. The colors of the outlets match those in Fig. 1

increase during the different particle release times is more significant when the aneurysm sac is present. The presence of the aneurysm sac makes the flow more complex, moreover, may have an effect of trapping particles for a longer time [26], therefore, the original simpler structures can become more filamentary and chaotic.

The P/A ratio as the function of the particle release time in both versions for the other cases is seen in Fig. 7. Generally, it is visible in most cases that the particle release time greatly affects the P/A ratio. It increases near the #3, #4 and #5 instances and decreases afterwards. The only exception is the red outlet. Since the red outlet is always the smallest one, only a small number of particles leave the domain through it. Therefore, the effect of a change is smaller as well. The exception to this is Case2, where the red outlet is not small, and the particle release time has an effect on the P/A ratio. It is worth noting that the P/A ratio can be large for a small outlet as well, since the relative area is in the denominator.

Similar to the previous conclusions, based on Fig. 6, the effect of an aneurysm is the same for the other four cases as well. The presence of an aneurysm sac increases the P/A ratio compared to the version without an aneurysm. Moreover, based on Case1 and Case4, it can be said that if the aneurysm is missing, the particle release time itself has less effect on the P/A ratio, and the peaks seem to be wider. The only exception is Case5, where there is only a slight difference between the two versions. The underlying reason may be that the size of the sac in this case is smaller, so it has a smaller effect if it is removed. In Case 4, the P/A ratio is larger in the version without the aneurysm sac but only for the red (smallest) outlet, but the other two outlets fit in line.

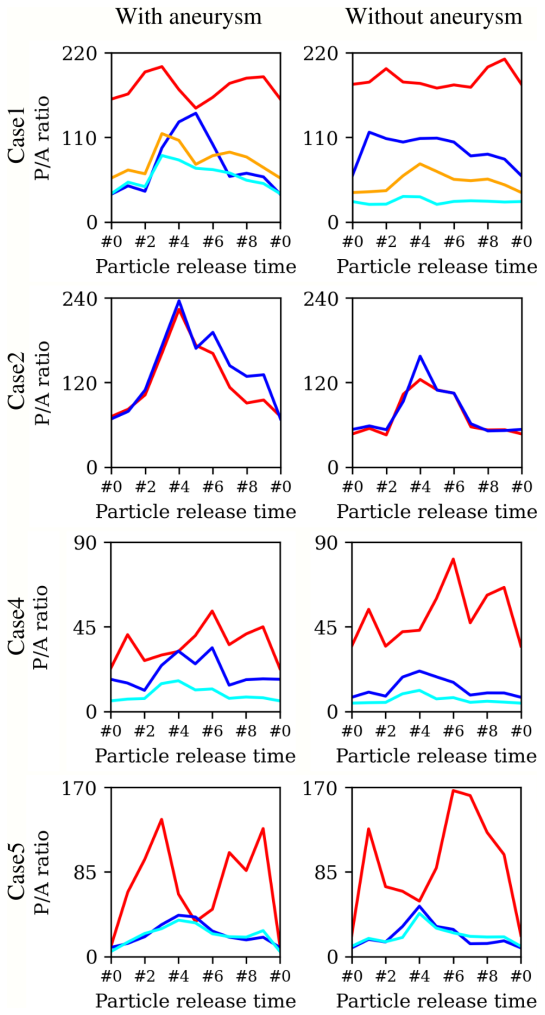

Fig. 7 Relative perimeter per relative area ratio for Case1, Case2, Case4 and Case5 with (left) and without aneurysm (right) as the function of particle release time. The colors of the outlets match those in Fig. 1

According to these results, it can be said that the particle release time is an essential factor to take into consideration in further projects dealing with particle paths. If targeted drug delivery is the aim, the heart cycle and the release time are influential parameters. It is important to note that the PRT is always high at the border of two neighboring regions corresponding to different outlets in Fig. 5. Inside one region, far from the boundary of it, the average particle leaves the observed domain in less than a heart cycle. However, particles released at the boundary of the regions corresponding to different outlets can take as much as a few seconds to leave the domain. The reason behind this phenomenon is that these particles reach the near-wall regions at the bifurcations, where they slow down. So if the nature of the particles is chaotic and filamentary, then the PRT is generally larger. Similarly, if an aneurysm develops on an artery, it can have a significant effect on the particles travelling in the blood. As the parameters have different effects in each case, a further study is planned, where more geometries will be investigated, and the P/A ratio differences will be correlated with geometrical parameters. Underlying reasons may be found based on a larger patient group.

3.3 Limitations

The most important limitation of the study is the wall handling of the lattice-Boltzmann method. Since the LBM uses a uniform grid which consists of cubes, the curved walls of the fluid domain are not fully followed, which may affect the particle paths. However, this limitation is partially solved by refining the uniform grid so the curves are followed more accurately. Furthermore, near-wall flow is slow, therefore, the particles are slow as well and may get stuck on the wall. This study concentrates on the particles released across the whole cross section, so the errors arising from near-wall effects are negligible.

Another limitation is the small sample size. Five aneurysm geometries are insufficient to derive definite conclusions about geometric parameters or the effect of the aneurysm sac. However, this research acts only as a preliminary study, and a further study is planned with a larger sample size based on the findings of this article, where correlations with geometric parameters (e.g. aneurysm size, ostium size, bifurcation angle, etc.) will be performed to further estimate the effects presented in this paper.

Lastly, the passive and massless assumption for the particles can be considered as a limitation as well. In real-life applications, small particles are not point-like, they have extents, so they have an effect, albeit small, on the flow. If their masses are taken into consideration as well, the particles would have inertia and would not take on the velocity of the flow instantaneously, and could drift outwards. However, the smaller the particles are, the better the assumptions are so that the particles can be considered to be massless and passive. In the future, these particles will represent physiological processes, then their characteristics will be modified accordingly.

The resolution-dependence of the perimeter was also not considered here because it was used only for comparison purposes.

4 Conclusions

The main goal of this research was to present a method to observe particle paths in real aneurysm geometries. The method is to process medical images, then obtain

the velocity field of the observed domain using the lattice-Boltzmann method, and finally, calculate the paths of passive and massless particles released in the flow. The paths, particularly the outlets through which the particle left the domain, are used to classify the points of the particle release plane. Each point of the plane is given an outlet number based on the path of the particle released from that point. Lastly, the relative perimeter, relative area and their ratio corresponding to an outlet were calculated.

The first part of this study was to investigate the effect of voxel resolution and the integrator time step size on the particle paths. Multiple simulations were performed with refined voxel size and time step size. Based on the Richardson extrapolation method, it was shown that 200 million total voxel number and dt = 1e-4 s integrator time step size is enough to accurately calculate the P/A ratio of the particles.

The second part of this research was to explore the effect of the removal of an aneurysm sac and the particle release time during the heart cycle on the particle paths. Five geometries were evaluated, and they confirmed that particle release time is an important factor. When the particles were still in the observed domain during the decelerating phase of the heart cycle, the paths became more chaotic and displayed a folded, filamentary structure on the release plane, and as a result the P/A ratio increased. The difference between the versions with and without the aneurysm sac showed that the aneurysm sac increases the chaotic nature.

The sample size of this study is limited, but these preliminary results imply that considering the aneurysm sac itself or the particle release time when calculating particle paths is an important finding. A more extensive study is planned with more patient-specific geometries in order to correlate the effect of P/A ratio changes with geometrical properties. Furthermore, physiological processes will also be taken into account into the characteristics of the particles.

Acknowledgement

This research was supported by the National Brain Research Program under the Contract Number 2017-1.2.1-NAP-2017-00002, and by the National Research, Development, and Innovation Fund of Hungary under Grant TKP2021-EGA-02.

References

[1] Blanco, P. J., Watanabe, S. M., Passos, M. A. R. F., Lemos, P. A., Feijóo, R. A. "An Anatomically Detailed Arterial Network Model for One-Dimensional Computational Hemodynamics", IEEE Transactions on Biomedical Engineering, 62(2), pp. 736–753, 2015. https://doi.org/10.1109/TBME.2014.2364522

[2] Wéber, R., Gyürki, D., Paál, G. "First blood: An efficient, hybrid one- and zero-dimensional, modular hemodynamic solver", International Journal for Numerical Methods in Biomedical Engineering, 39(5), e3701, 2023. https://doi.org/10.1002/cnm.3701

[3] Charlton, P. H., Harana, J. M., Vennin, S., Li, Y., Chowienczyk, P., Alastruey, J. "Modeling arterial pulse waves in healthy aging: a database for in silico evalution of hemodynamics and pulse wave indexes", American Journal of Physiology: Heart and Circulatory Physiology, 317(5), pp. H1062–H1085, 2019. https://doi.org/10.1152/ajpheart.00218.2019

[4] Blanco, P. J., Pivello, M. R., Urquiza, S. A., Feijóo, R. A. "On the potentialities of 3D-1D coupled models in hemodynamics simulations", Journal of Biomechanics, 42(7), pp. 919–930, 2009. https://doi.org/10.1016/j.jbiomech.2009.01.034

[5] Lopes, D., Puga, H., Teixeira, J., Lima, R. "Blood flow simulations in patient-specific geometries of the carotid artery: A systematic review", Journal of Biomechanics, 111, 110019, 2020. https://doi.org/10.1016/j.jbiomech.2020.110019

[6] Mendieta, J. B., Fontanarosa, D., Wang, J., Paritala, P. K., McGahan, T., Lloyd, T., Li, Z. "The importance of blood rheology in patient-specific computational fluid dynamics simulation of stenotic carotid arteries", Biomechanics and Modeling in Mechanobiology, 19(5), pp. 1477–1490, 2020. https://doi.org/10.1007/s10237-019-01282-7

[7] Paál, G., Ugron, Á., Szikora, I., Bojtár, I. "Flow in simplified and real models of intracranial aneurysms", International Journal of Heat and Fluid Flow, 28(4), pp. 653–664, 2007. https://doi.org/10.1016/j.ijheatfluidflow.2007.04.004

[8] Gasparotti, R., Liserre, R. "Intracranial aneurysms", European Radiology, 15(3), pp. 441–447, 2005. https://doi.org/10.1007/s00330-004-2614-8

[9] van Gijn, J., Rinkel, G. J. E. "Subarachnoid haemorrhage: diagnosis, causes and management", Brain, 124(2), pp. 249–278, 2001. https://doi.org/10.1093/brain/124.2.249

[10] Geers, A. J., Morales, H. G., Larrabide, I., Butakoff, C., Bijlenga, P., Frangi, A. F. "Wall shear stress at the initiation site of cerebral aneurysms", Biomechanics and Modeling in Mechanobiology, 16(1), pp. 97–115, 2017. https://doi.org/10.1007/s10237-016-0804-3

[11] Sunderland, K., Jiang, J. "Multivariate analysis of hemodynamic parameters on intracranial aneurysm initiation of the internal carotid artery", Medical Engineering & Physics, 74, pp. 129–136, 2019. https://doi.org/10.1016/j.medengphy.2019.09.010

[12] Kulcsár, Z., Ugron, Á., Marosfői, M., Berentei, Z., Paál, G., Szikora, I. "Hemodynamics of Cerebran Aneurysm Initiation: The Role of Wall Shear Stress and Spatial Wall Shear Stress Gradient", American Journal of Neuroradiology, 32(3), pp. 587–594, 2011. https://doi.org/10.3174/ajnr.A2339

[13] Csippa, B., Závodszky, G., Paál, G., Szikora, I. "A new hypothesis on the role of vessel topology in cerebral aneurysm initiation", Computers in Biology and Medicine, 103, pp. 244–251, 2018. https://doi.org/10.1016/j.compbiomed.2018.10.018

[14] Kulcsár, Z., Augsburger, L., Reymond, P., Pereira, V. M., Hirsch, S., Mallik, A. S., Millar, J., Wetzel, S. G., Wanke, I., Rüfenacht, D. A. "Flow diversion treatment: intra-aneurismal blood flow velocity and WSS reduction are parameters to predict aneurysm thrombosis", Acta Neurochirurgica, 154(10), pp. 1827–1834, 2012. https://doi.org/10.1007/s00701-012-1482-2

[15] Larrabide, I., Aguilar, M. L., Morales, H. G., Geers, A. J., Kulcsár, Z., Rüfenacht, D., Frangi, A. F. "Intra-Aneurysmal Pressure and Flow Changes Induced by Flow Diverters: Relation to Aneurysm Size and Shape", American Journal of Neuroradiology, 34(4), pp. 816–822, 2013. https://doi.org/10.3174/ajnr.A3288

[16] Závodszky, G., Csippa, B., Paál, G., Szikora, I. "A novel virtual flow diverter implantation method with realistic deployment mechanics and validated force response", International Journal for Numerical Methods in Biomedical Engineering, 36(6), e3340, 2020. https://doi.org/10.1002/cnm.3340

[17] Berg, P., Voß, S., Janiga, G., Saalfeld, S., Bergersen, A. W., Valen-Sendstad, K., Bruening, P., Goubergrits, L., Spuler, A., Chiu, T. L., On Tsang, A. C., …, Beuing, O. "Multiple Aneurysms AnaTomy Challenge 2018 (MATCH) –phase II: rupture risk assessment", International Journal of Computer Assisted Radiology and Surgery, 14(10), pp. 1795–1804, 2019. https://doi.org/10.1007/s11548-019-01986-2

[18] Qian, Y., Takao, H., Umezu, M., Murayama, Y. "Risk Analysis of Unruptured Aneurysms Using Computational Fluid Dynamics Technology: Preliminary Results", American Journal of Neuroradiology, 32(10), pp. 1948–1955, 2011. https://doi.org/10.3174/ajnr.A2655

[19] Leemans, E. L., Cornelissen, B. M. W., Rosalini, G., Verbaan, D., Schneiders, J. J., van den Berg, R., Vandertop, W. P., van Bavel, E. T., Slump, C. H., Majoie, C. B. L. M., Marquering, H. A. "Impact of Intracranial Aneurysm morphology and Rupture Status on the Particle Residence Time", Journal of Neuroimaging, 29(4), pp. 487–492, 2019. https://doi.org/10.1111/jon.12618

[20] Longest, P. W., Kleinstreuer, C. "Numerical simulation of Wall Shear Stress Conditions and Platelet Localization in Realistic End-to-Side Arterial Anastomoses", Journal of Biomechanical Engineering, 125(5), pp. 671–681, 2003. https://doi.org/10.1115/1.1613298

[21] Rayz, V. L., Boussel, L., Ge, L., Leach, J. R., Martin, A. J., Lawton, M. T., McCulloch, C., Saloner, D. "Flow residence time and regions of intraluminal thrombus deposition in intracranial aneurysms", Annals of Biomedical Engineering, 38(10), pp. 3058–3069, 2010. https://doi.org/10.1007/s10439-010-0065-8

[22] Shamloo, A., Forouzandehmehr, M. "Personalised deposition maps for micro- and nanoparticles targeting an atherosclerotic plaque: attributions to the receptor mediated adsorption on the inflamed endothelial cells", Biomechanics and Modeling in Mechanobiology, 18(3), pp. 813–828, 2019. https://doi.org/10.1007/s10237-018-01116-y

[23] Hewlin, R. L., Ciero, A., Kizito, J. P. "Development of a Two-Way Coupled Eulerian-Lagrangian Computational Magnetic Nanoparticle Targeting Model for Pulsatile Flow in a Patient-Specific Diseased Left Carotid Bifurcation Artery", Cardiovascular Engineering and Technology, 10(2), pp. 299–313, 2019. https://doi.org/10.1007/s13239-019-00411-8

[24] Meschi, S. S., Farghadan, A., Arzani, A. "Flow topology and targeted drug delivery in cardiovascular disease", Journal of Biomechanics, 119, 110307, 2021. https://doi.org/10.1016/j.jbiomech.2021.110307

[25] Schelin, A. B., Károlyi, G., de Mourna, A. P. S., Booth, N. A., Grebogi, C. "Chaotic advection in blood flow", Physical Review E: covering statistical, nonlinear, biological, and soft matter physics, 80(1), 016213, 2009. https://doi.org/10.1103/PhysRevE.80.016213

[26] Schelin, A. B., Károlyi, G., de Mourna, A. P. S., Booth, N. A., Grebogi, C. "Fractal structures in stenosis and aneurysms in blood vessels", Philosophical Transactions of the Royal Society A: Mathematical, Physical and Engineering Sciences, 368(1933), pp. 5605–5617, 2010. https://doi.org/10.1098/rsta.2010.0268

[27] Závodszky, G., Károlyi, G., Paál, G. "Emerging fractal patterns in a real 3D cerebral aneurysm", Journal of Theoretical Biology, 368, pp. 95–101, 2015. https://doi.org/10.1016/j.jtbi.2015.01.004

[28] Silva, I. M., Schelin, A. B., Viana, R. L., Caldas, I. L. "Transport of blood particles: Chaotic advection even in a healthy scenario", Chaos: An Interdisciplinary Journal of Nonlinear Science, 30(9), 093135, 2020. https://doi.org/10.1063/5.0013460

[29] Valen-Sendstad, K., Piccinelli, M., Steinman, D. A. "High-resolution computational fluid dynamics detects flow instabilities in the carotid siphon: Implications for aneurysm initiation and rupture?", Journal of Biomechanics, 47(12), pp. 3210–3216, 2014. https://doi.org/10.1016/j.jbiomech.2014.04.018

[30] Khan, M. O., Chnafa, C., Gallo, D., Molinari, F., Morbiducci, U., Steinman, D. A., Valen-Sendstad, K. "On the quantification and visualization of transient periodic instabilities in pulsatile flows", Journal of Biomechanics, 52, pp. 179–182, 2017. https://doi.org/10.1016/j.jbiomech.2016.12.037

[31] Suh, G.-Y., Les, A. S., Tenforde, A. S., Shadden, S. C., Spilker, R. L., Yeung, J. J., Cheng, C. P., Herfkens, R. J., Dalman, R. L., Taylor, C. A. "Quantification of Particle Residence Time in Abdominal Aortic Aneurysms Using Magnetic Resonance Imaging and Computational Fluid Dynamics", Annals of Biomedical Engineering, 39(2), pp. 864–883, 2011. https://doi.org/10.1007/s10439-010-0202-4

[32] Tambasco, M., Steinman, D. A. "On Assessing the Quality of Particle Tracking Through Computational Fluid Dynamic Models", Journal of Biomechanical Engineering, 124(2), pp. 166–175, 2002. https://doi.org/10.1115/1.1449489

[33] Hansen, K. B., Arzani, A., Shadden, S. C. "Finite element modeling of near-wall mass transport in cardiovascular flows", International Journal for Numerical Methods in Biomedical Engineering, 35(1), e3148, 2019. https://doi.org/10.1002/cnm.3148

[34] Kunov, M. J., Steinman, D. A., Ethier, C. R. "Particle volumetric residence time calculations in arterial geometries", Journal of Biomechanical Engineering, 118(2), pp. 158–164, 1996. https://doi.org/10.1115/1.2795954

[35] McIlhany, K. L., Wiggins, S. "Eulerian indicators under continuously varying conditions", Physics of Fluids, 24(7), 073601, 2012. https://doi.org/10.1063/1.4732152

[36] Reza, M. M. S., Arzani, A. "A critical comparison of different residence time measures in aneurysms", Journal of Biomechanics, 88, pp. 122–129, 2019. https://doi.org/10.1016/j.jbiomech.2019.03.028

[37] Gyürki, D., Szikora, I., Paál, G. "Calculating particle residence times in vessel geometries with aneurysm", In: Conference on Modelling Fluid Flow (CMFF'22), The 18th International Conference on Fluid Flow Technologies, Budapest, Hungary, 2022, pp. 290–295. ISBN 978-963-421-881-4

[38] Fedorov, A., Beichel, R., Kalpathy-Cramer, J., Finet, J., Fillion-Robin, J-C., Pujol, S., Bauer, C., Jennings, D., Fennessy, F., Sonka, M., Buatti, J., … Kikinis, R. "3D Slicer as an Image Computing Platform for the Quantitative Imaging Network", Magnetic Resonance Imaging, 30(9), pp. 1323–1341, 2012. https://doi.org/10.1016/j.mri.2012.05.001

[39] Cignoni, P., Callieri, M., Corsini, M., Dellepiane, M., Ganovelli, F., Ranzuglia, G. "MeshLab: an Open-Source Mesh Processing Tool", In: Sixth Eurographics Italian Chapter Conference, pp. 129–136, 2008. ISBN 978-3-905673-68-5 https://doi.org/10.2312/LocalChapterEvents/ItalChap/ItalianChapConf2008/129-136

[40] Ugron, Á., Farinas, M-I., Kiss, L., Paál, G. "Unsteady velocity measurements in a realistic intracranial aneurysm model", Experiments in Fluids, 52(1), pp. 37–52, 2012. https://doi.org/10.1007/s00348-011-1206-z

[41] Chnafa, C., Brina, O., Pereira, V. M., Steinman, D. A. "Better Than Nothing: A Rational Approach for Minimizing the Impact of Outflow Strategy on Cerebrovascular Simulations", American Journal of Neuroradiology, 39(2), pp. 337–343, 2018. https://doi.org/10.3174/ajnr.A5484

[42] Latt, J., Malaspinas, O., Kontaxakis, D., Parmigiani, A., Lagrava, D., Brogi, F., Belgacem, M. B., Thorimbert, Y., Leclaire, S., Li, S., Marson, F., … Chopard, B. "Palabos: Parallel Lattice Boltzmann Solver", Computers & Mathematics with Applications, 81, pp. 334–350, 2021. https://doi.org/10.1016/j.camwa.2020.03.022

[43] Noble, D. R., Georgiadis, J. G., Buckius, R. O. "Comparison of accuracy and performance for lattice Boltzmann and finite difference simulations of steady viscous flow", 23(1), pp. 1–18, 1996. https://doi.org/10.1002/(SICI)1097-0363(19960715)23:1<1::AID-FLD404>3.0.CO;2-V

[44] Breuer, M., Bernsdorf, J., Zeiser, T., Durst, F. "Accurate computations of the laminar flow past a square cylinder based on two different methods: lattice-Boltzmann and finie-volume", International Journal of Heat and Fluid Flow, 21(2), pp. 186–196, 2000. https://doi.org/10.1016/S0142-727X(99)00081-8

[45] Závodszky, G., Paál, G. "Validation of a lattice Boltzmann method implementation for a 3D transient fluid flow in an intracranial aneurysm geometry", International Journal of Heat and Fluid Flow, 44, pp. 276–283, 2013. https://doi.org/10.1016/j.ijheatfluidflow.2013.06.008

[46] Celik, I. B., Ghia, U., Roache, P. J., Freitas, C. J., Coleman, H., Raad, P. E. "Procedure for Estimation and Reporting of Uncertainty Due to Discretization in CFD Applications", Journal of Fluids Engineering, 130(7), 078001, 2008. https://doi.org/10.1115/1.2960953